Facile Insertion of Lithium into Nanocrystalline $AlNbO_4$ at Room Temperature

M. Anji Reddy and U. V. Varadaraju

Material Science Research Centre and Department of Chemistry, Indian Institute of Technology Madras, Chennai 600 036, India

Received May 1, 2008
Revised Manuscript Received June 10, 2008

Recently, nanometer-sized materials generated interest with respect to lithium insertion/extraction reactions, because of their high reactivity compared to the bulk analogues.[1–15] Micrometer-sized particles seem to impose limitations on the lithium insertion/extraction reactions, ascribable to large diffusion path lengths and strain associated with insertion reactions. Using nanometer-sized particles, such constraints can be mitigated. The best examples to describe such effects are α-Fe_2O_3,[2] anatase TiO_2, [3,4] and recently proposed rutile type TiO_2,[5–8] MnO_2,[9,10] and VO_2,[11] brookite TiO_2,[12–14] and pseudo brookite $MgTi_2O_5$.[15] Although insertion of Li into 0.5 μm particles of α-Fe_2O_3 is insignificant (0.05Li/f.u.), 1Li/Fe_2O_3 can be inserted into 20 nm size particles.[2] In the case of rutile TiO_2, 1Li/TiO_2 can be inserted in nanocrystalline TiO_2 at RT vis a vis 0.03−0.3Li/TiO_2 into bulk samples. Similar influence of particle size and nanostructuring on Li insertion was demonstrated in all the above-mentioned compounds. The high reactivity found at the nanolevel opens the possibility of finding new and novel Li insertion hosts. Study of compounds with various crystal structures and electroactive elements present in the lattice for Li insertion/extraction is an urgent need to pave the way for understanding the behavior of the nanocrystalline state. The present study assumes importance in this context. Here, we report our studies on the channel compound, $AlNbO_4$, wherein we demonstrate significant Li uptake in the nanocrystalline form vis a vis the bulk form.

Figure S1 shows the crystal structure view of $AlNbO_4$ in the ac plane (see the Supporting Information).[16] $AlNbO_4$ is isostructural with VO_2 (B). The compound crystallizes in monoclinic space group *C*2/*m* (12) with lattice parameters $a = 12.15$ Å, $b = 3.734$ Å, $c = 6.488$ Å, and $\beta = 107.61$. The structure is built-up of AlO_6 and NbO_6 octahedra. There are two types of octahedra present in the structure (shown in Figure S1 of the Supporting Information). Type 1 octahedra share five edges and type 2 share four edges. The type 1 octahedra are occupied predominantly by Al and the type 2 are occupied predominantly by Nb. The typical cation distributions are 0.81(Al)/0.19(Nb) in type1 and 0.19(Al)/0.81(Nb) in type 2.[17] The structure of $AlNbO_4$ can also be described as a 2 × 2 shear structure of ReO_3. Murphy et al.[18] studied chemical lithium insertion into $AlNbO_4$. Their studies show that using *n*-butyl lithium, 0.44Li/$AlNbO_4$ and 3Li/$AlNbO_4$ are inserted at RT and at 50 °C, respectively. However, later studies by Zachau-Christiansen et al.,[19] have shown that chemically, insertion of only 0.1Li/$AlNbO_4$ can be affected at RT; on the other hand, up to 2Li/$AlNbO_4$ can be inserted electro-chemically at 100 °C in polymer electrolyte cells. These studies show that lithium insertion is indeed possible; sluggish kinetics prevent lithium insertion into $AlNbO_4$ at RT. Thus, in analogy with rutile TiO_2 it should be possible to achieve high lithium insertion activity at RT by reducing the crystallite size to a few nanometers.

Micrometer-sized and nanometer-sized samples of $AlNbO_4$ were prepared by the conventional solid state reaction (SSR) and polymerizable complex (PC) method respectively (see the Supporting Information). Figure 1a presents the powder XRD patterns of $AlNbO_4$ synthesized by SSR and PC methods. All the peaks in both the XRD patterns are indexed according to the JCPDS card no. 41−0347. Phase pure samples are obtained by both the methods. The calculated lattice parameters are $a = 12.1577(3)$, $b = 3.7392(1)$, $c = 6.4895(2)$ and $a = 12.154(2)$, $b = 3.7342(5)$, $c = 6.4947(9)$ for phases synthesized by SSR and PC methods, respectively. The mean crystallite size of $AlNbO_4$ synthesized by PC method is calculated from the XRD pattern using the Scherrer formula. The obtained value is 17nm. Figure 1b shows the SEM image of the sample prepared by SSR; the particle size is in the range 1−2 μm. Figure 1c shows the TEM image of the sample synthesized PC method and Figure 1d shows the HRTEM image of a single crystallite (∼15 nm). In the case of the PC method, the crystallites are aggregated and the crystallite size is in the range 15−20 nm.

* Corresponding author. E-mail: varada@iitm.ac.in.

(1) Arico, A. S.; Bruce, P.; Scrosati, B.; Tarascon, J.-M.; Van Schalkwijki, W. *Nat. Mater.* **2005**, *4*, 366.
(2) Larcher, D.; Masquelier, C.; Bonnin, D.; Chabre, Y.; Masson, V.; Leriche, J. -B.; Tarascon, J.-M. *J. Electrochem. Soc.* **2003**, *150*, A133.
(3) Sudant, G.; Baudrin, E.; Larcher, D.; Tarascon, J.-M. *J. Mater. Chem.* **2005**, *15* (12), 1263.
(4) Wagemaker, M.; Borghols, W. J. H.; Mulder, F. M. *J. Am. Chem. Soc.* **2007**, *129* (14), 4323.
(5) Hu, Y.-S.; Kienle, L.; Guo, Y.-G.; Maier, J. *Adv. Mater.* **2006**, *18*, 1421.
(6) Anji Reddy, M.; Satya Kishore, M.; Pralong, V.; Caignaert, V.; Varadaraju, U. V.; Raveau, B. *Electrochem. Commun.* **2006**, *8*, 1299.
(7) Baudrin, E.; Cassaignon, S.; Koelsch, M.; Jolivet, J.-P.; Dupont, L.; Tarascon, J. -M. *Electrochem. Commun.* **2007**, *9*, 337.
(8) Jiang, C.; Honma, I.; Kudo, T.; Zhou, H. *Electrochem. Solid-State Lett.* **2007**, *10*, A127.
(9) Luo, J.-Y.; Zhang, J. -J.; Xia, Y. -Y. *Chem. Mater.* **2006**, *18*, 5618.
(10) Jiao, F.; Bruce, P. G. *Adv. Mater.* **2007**, *19*, 657.
(11) Muñoz-Rojas, D.; Baudrin, E. *Solid State Ionics.* **2007**, *178*, 1268–1273.
(12) Anji Reddy, M.; Satya Kishore, M.; Pralong, V.; Varadaraju, U. V.; Raveau, B. *Electrochem. Solid-State Lett.* **2007**, *10*, A29.
(13) Kim, D.- W.; Lee, D.-H.; Park, J.-G.; Choi, K. J.; Choi, H.-J. *Eur. J. Inorg. Chem.* **2008**, *6*, 878.
(14) Anji Reddy, M.; Pralong, V.; Varadaraju, U. V.; Raveau, B. *Electrochem. Solid-State Lett.* **2008**, *11*, A132.
(15) Anji Reddy, M.; Satya Kishore, M.; Pralong, V.; Caignaert, V.; Varadaraju, U. V.; Raveau, B. *Chem. Mater.* **2008**, *20*, 2192.
(16) Pedersen, B. F. *Acta Chem. Scand.* **1962**, *16*, 421.
(17) Greis, O.; Ziel, R.; Garcia, D. E.; Claussen, N.; Breidenstein, B.; Haase, A. *Mater. Sci. Forum.* **1996**, 228–231; Pt. 2, European Powder Diffraction.
(18) Murphy, D. W.; Greenblatt, M.; Cava, R. J.; Zahurak, S. M. *Solid State Ionics* **1981**, *5*, 327.
(19) Zachau-Christiansen, B.; West, K.; Jacobsen, T.; Skaarup, S. *Solid State Ionics* **1992**, *53−56*, 364.

10.1021/cm801194b CCC: $40.75
Published on Web 06/27/2008

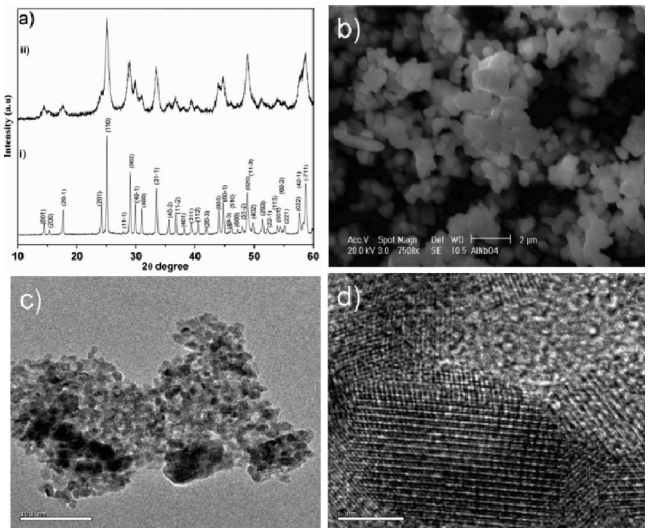

Figure 1. (a) PXRD pattern of (i) synthesized by SSR and (ii) PCM, (b) SEM image of sample prepared by SSR (scale bar 2 μm), (c) TEM image of the sample synthesized by PCM (scale bar 100 nm), and (d) HRTEM image showing a typical crystallite (scale bar 5 nm).

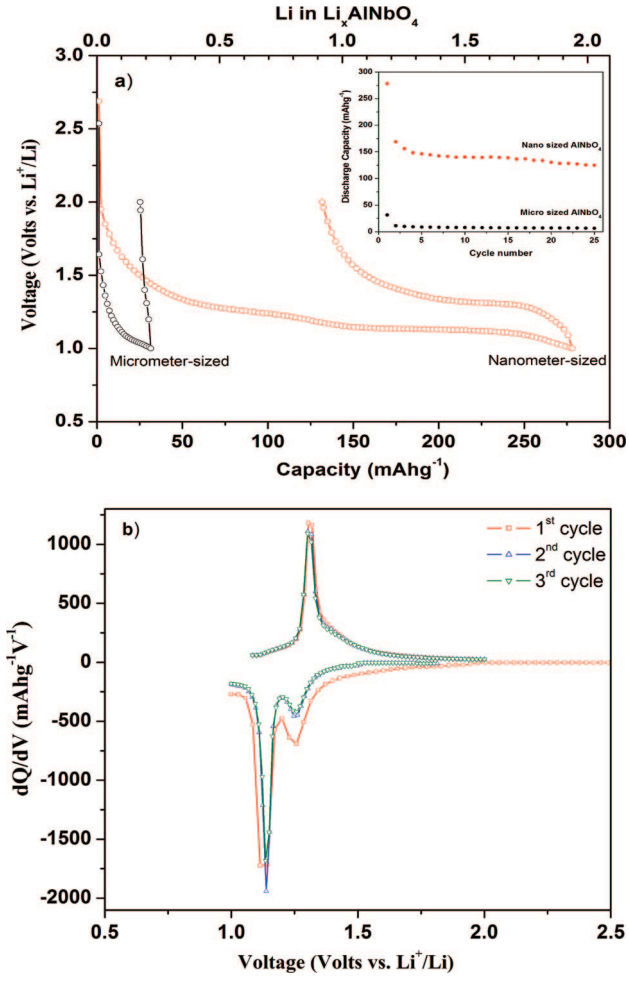

Figure 2. (a) Voltage−composition profiles of micrometer- and nanometer-sized $AlNbO_4$ (obtained at 14 mA g^{-1}), inset shows the cycling behavior; (b) corresponding differential capacity plot for the first three cycles.

Figure 2a shows the voltage-composition profiles of micro and nanometer-sized $AlNbO_4$. The charge−discharge curves are obtained by passing a constant current of 14 mA g^{-1}. The difference in the lithium insertion behavior between the micrometer-sized and nanometer-sized samples is evident. In the case of the micrometer-sized sample, insertion of only 0.22 Li/$AlNbO_4$ is observed. The low electroactivity of $AlNbO_4$ at RT is in line with the earlier observations.[18,19] In contrast, in the case of nanometer-sized sample, the electroactivity is remarkably higher; 1.9Li/$AlNbO_4$ are inserted when discharged to 1.0 V and 1Li/$AlNbO_4$ are extracted upon charge to 2.0 V. The discharge profile of nanometer-sized sample can be divided into three regions. The three regions can be clearly seen as peaks in the differential capacity plot (shown in Figure 2b). In the first region, 2.0−1.3V, the voltage varies smoothly with Li content, indicative of solid solution behavior, and corresponds to the insertion of 0.5Li. In the second region, 1.3−1.15 V, 0.5Li are inserted at an average voltage of 1.25 V. In the third region, 1.15−1V, 0.9Li are inserted at 1.13 V. The second and third regions exhibit a plateaulike behavior and the plateaus are attributed to the biphasic nature of the insertion process. Cava et al.,[21] studied chemical lithium insertion into FeV_3O_8 with TiO_2 (B) structure using *n*-butyl lithium. They observed that 2Li can be inserted at RT. The TiO_2 (B) structure has tetra capped cavities with four inequivalent (2 + 2) five-coordinated square pyramidal sites. Chemical insertion of Li leads to occupancy of two equivalent sites out of the four sites available (corresponding to the composition of $Li_2FeV_3O_8$ for the daughter phase), the other two equivalent sites being unoccupied. In the present study, we are able to fill all four sites in the nanocrystalline $AlNbO_4$, resulting in the phase Li_2AlNbO_4. With the two available sites for Li occupation being crystallographically inequivalent but with similar geometries, it is reasonable to expect that the site energies are only slightly different. Hence, one would expect two plateaus at slightly different voltages in the voltage vs capacity plots. Indeed, this is observed in the present study. The end of the first plateau corresponds to the composition $LiAlNbO_4$ and the end of second plateau corresponds to the composition $Li_{1.9}AlNbO_4$ (Li_2AlNbO_4 from GITT studies (Figure 3)). A similar two-step behavior is observed in the electrochemical insertion of Li into TiO_2 (B) and VO_2 (B).[22] In addition, the solid solution range (0.5Li/$AlNbO_4$) observed in the present study agrees well with that of VO_2 (B).[22] Murphy et al. found changes in lattice parameters of $AlNbO_4$ upon Li insertion.[18] The peaks in the XRD patterns, in the present study, are broad due to the nanocrystalline nature of the sample and are further broadened by the RT insertion reaction. Hence, shifts in peak positions of the lithiated phases vis a vis the parent phase are not discernible.

During charge, 1Li is extracted at an average potential of 1.3V. A large irreversible capacity loss (ICL) of 0.9Li is seen in the first cycle, suggesting complete extraction of Li is difficult. A rather large ICL is also seen in micrometer-sized $AlNbO_4$ studied at 100 °C.[19] The reasons for the large ICL are not known at present. Despite the high ICL in the

(20) Zhou, Y.; Qiu, Z.; Lu, M.; Ma, Q.; Zhang, A.; Zhou, G.; Zhang, H.; Yang, Z. *J. Phys. Chem. C* **2007**, *111*, 10190.
(21) Cava, R. J.; Santoro, A.; Murphy, D. W.; Zahurak, S.; Roth, R. S. *J. Solid State Chem.* **1983**, *48*, 309.
(22) Baudrin, E.; Sudant, G.; Larcher, D.; Dunn, B.; Tarascon, J. M. *Chem. Mater.* **2006**, *18*, 4369.

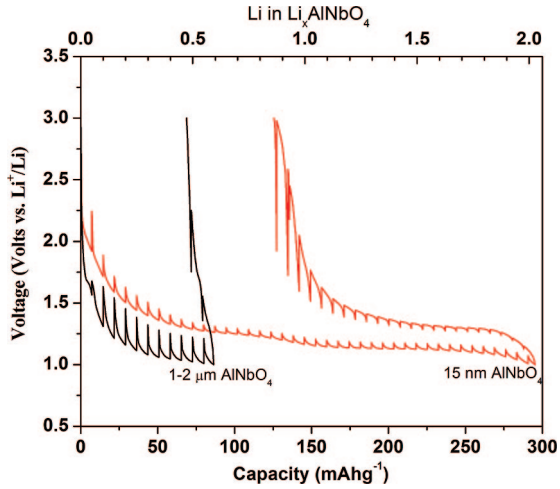

Figure 3. Galvanostatic intermittent titration technique (GITT) curve of micrometer- and nanometer-sized $AlNbO_4$ (obtained at 7 mA g^{-1}).

first cycle, the nanocrystalline phase shows good reversibility on further cycling. 0.9Li are reversibly inserted even after 25 cycles (inset of Figure 2a). As evident from the differential capacity plot (Figure 2b), during second and third discharge−charge cycles, Li insertion/extraction occurs at potentials similar to those observed in the first cycle. This further suggests that there are no major structural changes during first and subsequent Li insertion/extraction cycles. The electrochemical behavior of nanometer-sized $AlNbO_4$ studied here is similar to that of micrometer-sized $AlNbO_4$ studied at 100 °C.[19]

If diffusion of Li from the surface to the bulk of the crystallite is sluggish, Li accumulates on the surface of the crystallite. Thus, the surface of the crystallite attains its maximum capacity before the bulk of the material. Consequently, the material delivers less capacity than its ability. This often occurs when high current rates are used. Hence, we performed a galvanostatic intermittent titration technique (GITT) experiment on $AlNbO_4$ in order to ascertain the C rate dependence of Li insertion and also to ascertain the equilibrium insertion potential. Figure 3 shows the GITT curves of both micrometer- and nanometer-sized $AlNbO_4$. The charge−discharge curves are obtained by passing a constant current of 7 mA g^{-1} (∼*C*/20 rate) for 1 h and resting the cell for 2 h. Interestingly, in GITT mode, 0.59Li/$AlNbO_4$ are inserted in the micrometer-sized sample, a significant improvement over 0.22Li/$AlNbO_4$ at a *C*/10 rate. In the case of nanometer-sized sample, 2.0Li/$AlNbO_4$ are inserted; 0.1Li more compared to 1.9Li at *C*/10 rate. Upon charge to 3.0 V, 1.16Li are extracted. As it is evident that the amount of Li inserted is largely dependent on the rate of Li insertion for micrometer-sized sample, we performed discharge−charge at a *C*/100 (1.4 mA g^{-1}) (see Supporting Information, Figure S2) rate to get further insight into insertion behavior. A substantially large amount of 1.3Li/$AlNbO_4$ are inserted and 0.3Li are extracted (however, such low rates are practically of limited use). This suggests that the observed low Li insertion activity of micrometer-sized $AlNbO_4$ is largely due to the sluggish diffusion of lithium in the structure. In contrast, large amount of lithium is inserted at much higher rates in case of nanometer-sized $AlNbO_4$, because the nanocrystalline phases have shorter diffusion path lengths. Thus, crystallite size plays a crucial role in determining the electroactivity of $AlNbO_4$ under ambient conditions.

In conclusion, the following interesting features of Li insertion in $AlNbO_4$ emerge. The high theoretical specific capacity of 291 mA h g^{-1} (assuming the redox couple of Nb^{5+}/Nb^{3+} which requires insertion of 2Li into the structure) can be realized in nanocrystalline form. The insertion/extraction process occurs at almost a flat potential of ∼1.2 V vs Li with low polarization between charge and discharge. The reversible capacity is 130 mA h g^{-1}. All these features make nanocrystalline $AlNbO_4$ a compound of immense interest as negative electrode material in Li-ion batteries. Further improvement in reversible capacity is possible. It is known that even in the nano regime, the crystallite size has strong influence on reversible capacity as we demonstrated in nanocrystalline brookite TiO_2.[14] Thus, we conceive that in the case of $AlNbO_4$, by reducing the crystallite size further, the ICL can be minimized thereby, increasing the reversible capacity. Such studies are currently underway in our laboratory.

Supporting Information Available: Crystal structure view, materials synthesis, electrode fabrication and other details, and voltage−composition profile of micrometer-sized $AlNbO_4$ (PDF). This information is available free of charge via the Internet at http://pubs.acs.org.

CM801194B